Nonstoichiometric Salt Intercalation as a Means to Stabilize Alkali Doping of 2D Materials

Yuanxi Wang,[1,2] Vincent H. Crespi,[1,3] Marvin L. Cohen,[4,5] and Amir Nourhani[6,7,8,*]
[1]2-Dimensional Crystal Consortium, Materials Research Institute, The Pennsylvania State University, University Park, Pennsylvania 16802, USA
[2]Department of Physics, University of North Texas, Denton, Texas 76201, USA
[3]Department of Physics, The Pennsylvania State University, University Park, Pennsylvania 16802, USA
[4]Department of Physics, University of California at Berkeley, Berkeley, California 94720, USA
[5]Materials Sciences Division, Lawrence Berkeley National Laboratory, Berkeley, California 94720, USA
[6]Department of Mechanical Engineering, University of Akron, Akron, Ohio 44325, USA
[7]Biomimicry Research and Innovation Center, University of Akron, Akron, Ohio 44325, USA
[8]Departments of Biology, Mathematics, and Chemical, Biomolecular, and Corrosion Engineering, University of Akron, Akron, Ohio 44325, USA

(Received 1 March 2021; revised 11 August 2022; accepted 30 September 2022; published 23 December 2022)

Although doping with alkali atoms is a powerful technique for introducing charge carriers into physical systems, the resulting charge-transfer systems are generally not air stable. Here we describe computationally a strategy towards increasing the stability of alkali-doped materials that employs stoichiometrically unbalanced salt crystals with excess cations (which could be deposited during, e.g., *in situ* gating) to achieve doping levels similar to those attained by pure alkali metal doping. The crystalline interior of the salt crystal acts as a template to stabilize the excess dopant atoms against oxidation and deintercalation, which otherwise would be highly favorable. We characterize this doping method for graphene, $NbSe_2$, and Bi_2Se_3 and its effect on direct-to-indirect band gap transitions, 2D superconductivity, and thermoelectric performance. Salt intercalation should be generally applicable to systems which can accommodate this "ionic crystal" doping (and particularly favorable when geometrical packing constraints favor nonstoichiometry).

DOI: 10.1103/PhysRevLett.129.266401

Charge-transfer doping from alkali metals to low-dimensional materials—whether to quasi-0D fullerenes [1–3], 1D nanotubes [4,5], 2D dichalcogenides [6,7], graphene [8,31,33,34], or layered graphite [9,10]—can introduce high carrier densities into systems with both strong covalent bonding and relatively weak intermolecular or intersheet interaction. In zero dimensions, the high density of electronic states produced by weak intermolecular overlap yields high superconducting transition temperatures [11,12]. In 1D, doped carbon nanotubes provide highly conductive channels [13]. Well-known cases in higher dimensions include alkali-intercalated graphite as electrodes for energy storage and lithium-intercalated layered dichalcogenides as switchable phase-change devices [14]. Unfortunately, all these systems suffer from the air sensitivity of alkali metal; most must be studied under inert atmospheres. We present a strategy to potentially increase the stability of alkali-metal intercalants, using nonstoichiometric salt with excess alkali instead of pure alkali metals. The presence of the stoichiometric salt "backbone" to which the excess alkali is attached (Fig. 1 left panel) may improve the thermodynamic and kinetic stability of the alkali metal against oxidation or deintercalation [15,16], while preserving its ability to donate electrons to an adjacent 2D sheet. We then show how this same method of "salted intercalation" can decouple various layered materials (e.g., $NbSe_2$ and Bi_2Se_3) to recover monolayerlike behavior in bulk systems.

For intercalation into bilayer graphene, we first focus on potassium iodide (KI), since its (111) facet has a metal atom areal density close to that of KC_8 [17] (Fig. 1, right panel) and since iodine is imaged relatively easily in transmission electron microscopy [18]. We compare the stability of these non-stoichiometric salt slabs exposing (111) surfaces with many other possible intercalating phases with different

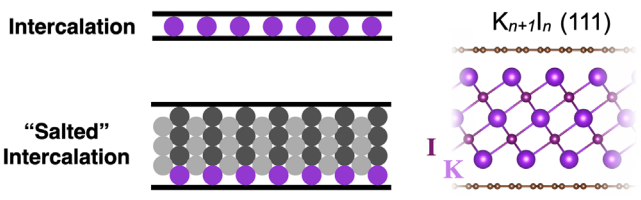

FIG. 1. (Left) The thermodynamic and kinetic stability of a graphitic (or other 2D) system doped by intercalating alkali metal can be modified by the presence of an adjacent "backbone" salt crystal that templates the excess alkali or halogen atoms, as shown by (right) the side view of a K_3I_2 system.

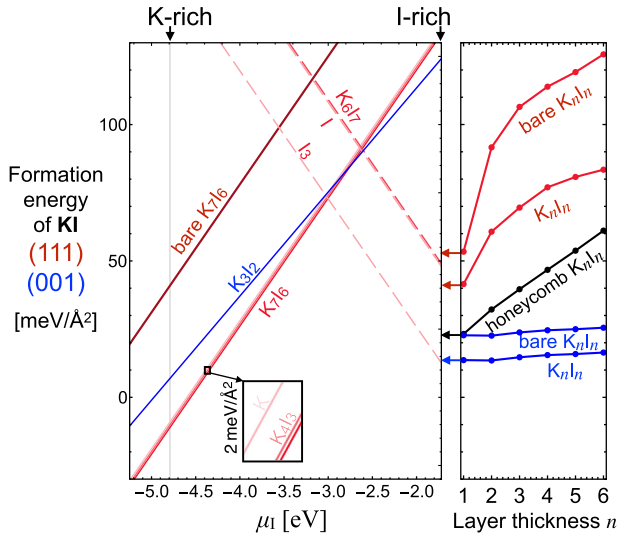

FIG. 2. (Left) Formation energies for intercalated KI slabs with (111) (red) or (001) (blue) terminations. Systems with excess K and excess I are, respectively, plotted in solid and dashed lines. (Right) Thickness dependent formation energies for three stoichiometric K_nI_n phases—the cubic (111) phase in red, the (001) phase in blue (with and without graphene caps), and the honeycomb phase in black.

crystal facets and terminations, including a (001) phase, a stoichiometric (111) phase, and a honeycomb phase [19–22] (see Fig. S1 in Supplemental Material [23]). The rocksalt (111) planes alternate in alkali/halogen composition, so for an odd number of layers, e.g., $K_{n\pm1}I_nC_x$ (x is the carbon stoichiometry of the graphene caps), there is a stoichiometric excess of one alkali or halogen layer. The $5.00:2.46 \approx 2:1$ near commensuration between the in-plane lattices of KI(111) and graphene allows for a small 2×2 graphene $+ 1\times1$ KI(111) supercell. For the other incommensurate KI systems, we use $3\times5\sqrt{3}$ graphene $+$ $\sqrt{2}\times3\sqrt{2}$ KI(001) and 7×7 graphene $+ 3\times3$ honeycomb-KI. All supercell choices ensure residual in-plain strains below 3%. See Supplemental Material [23] for details on all density functional theory calculations and supercell geometries.

KI.—We first assess the thermodynamic stability of intercalated KI exposing (111) or (001) facets. We evaluate thermodynamic stabilities from the formation energies $E_{K_mI_nC_x} - x\mu_C - m\mu_{KI} + (m-n)\mu_I$ per unit area, where μ_{KI} and μ_C are the free energies per KI and C taken, respectively, from the total energies of bulk KI and graphene; μ_I is the iodine chemical potential. All μ_I-dependent formation energies are plotted in the left panel of Fig. 2, while the μ_I-independent ones ($m = n$) in the right panel are plotted as a function of layer thickness. The latter include stoichiometric K_nI_n slabs exposing (001) facets in blue, and K_nI_n exposing (111) facets in red. All structures are capped with graphene on both sides unless their names are prefaced with "bare." The K- and I-rich limits are determined by setting $\mu_I = E_{I_2}/2$ and $\mu_I = \mu_{KI} - E_{\text{bulk-K}}$ and are indicated by black vertical arrows. Doing so assumes equilibrium with bulk KI, and that μ_K and μ_I are constrained by their sum $\mu_K + \mu_I = \mu_{KI}$.

For the majority of the allowed μ_I (between -4.1 and -1.9 eV), the stoichiometric K_nI_n exposing the nonpolar (001) facet is, not surprisingly, energetically favored against any other phase, and can be further stabilized by 10 meV/Å^2 through bilayer graphene encapsulation, as shown by the two nearly flat blue curves in the right panel. The same stabilization presumably drives intercalation of alkali metal halide salts into carbon nanotubes [40,41]. The nonstoichiometric $K_{n+1}I_n$ (001) facet (blue solid line in left panel, with one layer of K added to a (001) surface of K_2I_2) is relatively unstable at any μ_I. For lower μ_I, the family of $K_{n+1}I_n$ (111) becomes preferred; its formation energies are essentially the same (within 2 meV/Å^2) for different n, including $n = 0$, as shown magnified in Fig. 2 inset for $K_1I_0 = K$, K_4I_3, and K_7I_6. The similar thermodynamic stabilities with ($n = 0$) or without salt backbones ($n > 0$) is not surprising, since complete charge transfer to graphene occurs as long as K is in excess. The band structures and Fermi levels of a salt-intercalated $K_7I_6C_{16}$ and K-intercalated KC_{16} in Fig. 3(a) are nearly identical, with Fermi levels ~1.2 eV above the Dirac point for all excess K cases, except for the addition of halogen- and alkali-derived bands below and above the Fermi energy in the slab case. The calculated work function after K_7I_6 doping decreases to 3.3 eV from the 4.4 eV of graphene, a trend similar to the reported work function decrease to 2.7 and 2.8 eV in nonstoichiometric NaCl and NaI intercalated graphite systems [42], where the smaller work function is presumably due to higher areal densities of excess Na.

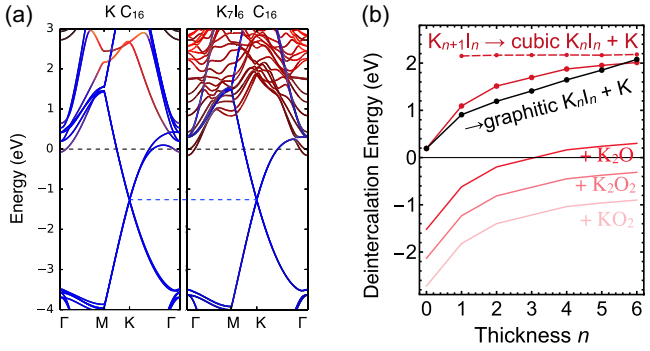

FIG. 3. (a) Band structure of electron-doped graphene bilayers (KC_{16} and $K_7I_6C_{16}$). Fermi levels are set to zero. Colored bands indicate projection of total wave function onto K (warm colors) and C orbitals (blue), respectively. (b) The curves with points show deintercalation energies for $K_{n+1}I_n \to K_nI_n +$ bulk metal K per deintercalated K atom, where the K_nI_n end state is the cubic (111) phase (red) or the honeycomb phase (black). Curves without points are deintercalation energies for potassium oxide end states.

The similar stabilities regardless of salt backbones are not problematic for the experimental realization of $K_{n+1}I_n$ because the above calculations assumed equilibration with bulk KI: one can devise a system out of equilibrium where KI dissolves and is transported towards KC_8 where KI recrystalizes, nucleating where there are already metal atoms and forming $K_{n+1}I_n$. In fact, Refs. [42,43] introduced a mixture of alkali metal and alkali halides (or oxides) to achieve a "salted" intercalation, with a surprising lattice match between graphite and the intercalants even for Na salts, despite generating ~7% strain. The paucity of observations of stand-alone nonstoichiometric salt (i.e., without charge transfer to a nearby acceptor or donor) may be attributed to the instability of this phase without graphene encapsulation due to the not-fully ionized K surface, as shown by the same-slope line in dark red for bare K_7I_6.

To thoroughly investigate possible low-energy KI phases, we discuss a final group of potential competing phases before advancing to assess the air stability of $K_{n+1}I_n$. Returning to the right panel of Fig. 2, we consider stoichiometric K_nI_n (111) phases, where the energies of the $n = 1$–6 cases with and without graphene caps are plotted in red. The lowest energies for each case are for $n = 1$ and are aligned with the left plot by red arrows. These K_nI_n systems are strongly destabilized by the huge out-of-plane dipole moment built up from the alternating K and I planes [38]; the screening from the encapsulating bilayer graphene partially relieves this instability but still leaves this phase unfavorable in the entire μ_I range considered. These interesting polar phases may be stabilized in a vertical electric field. For sufficiently thin layers ($n < 9$ [19]), the ground state of K_nI_n (111) becomes a layered honeycomb structure (black in Fig. 2 right panel) instead of cubic to reduce the vertical dipole moment. The $n = 1$ case is marked by a black arrow; this single-layer honeycomb KI expands its in-plane lattice constant from 4.86 to 5.87 Å and becomes almost as stable as bare KI (001) nonpolar surface (blue in Fig. 2 right panel). For larger n, the energies of honeycomb and cubic (111) K_nI_n crosses over, due to the smaller surface energy but larger bulk energy for the honeycomb phase.

In view of the above analysis, three potential low-energy phases of KI (111) are: for low μ_I, nonstoichiometric $K_{n+1}I_n$; for intermediate μ_I, honeycomb K_nI_n for thinner and cubic uncompensated K_nI_n for thicker salt layers. A fourth phase dominating high μ_I, intercalated I_3, is discussed in the Supplemental Material [23]. These four K_nI_n phases are focused on below as the products of deintercalation. The nonpolar (001) phase, although having a μ_I-independent lowest energy, will be excluded in the following discussion on deintercalation products of a $K_{n+1}I_n$ (111) since a thick K_nI_n (111) structure would unlikely transform into K_nI_n (001) without undergoing substantial deformation (with a high kinetic barrier) inside bilayer graphene, whereas relaxing it into honeycomb K_nI_n only requires overcoming a barrier of less than 0.1 eV [19].

Deintercalation.—The key quantity in characterizing air stability is not stability with respect to bulk KI at a chosen μ_I, but stability of an already-formed $K_{n+1}I_n$ against oxidized potassium. Deintercalation energetics are determined by the oxidation state of the deintercalated K. We first examine $K_{n+1}I_n \rightarrow K_nI_n +$ bulk metal K to inspect general trends from the contribution of the salt "backbone" to the kinetic stability against deintercalation and then extend the results to potassium oxides.

As shown in Fig. 3(b), for both K_nI_n end states in the honeycomb phase and cubic (111) phase (both still including graphene caps), the per-atom energy penalty of deintercalating K increases with increasing n due to the increasing instability of K_nI_n. For the honeycomb case (black), the deintercalation energy increases linearly due to the linearly increasing bulk energy of honeycomb K_nI_n. For the cubic K_nI_n case (red), the deintercalation energy saturates at 2.1 eV due to graphene screening and charge transfer from one interface to the other. The asymptote can be alternatively obtained from another process (not involving any structures with dipoles) that converges faster with n: Taking half the deintercalation energy of $K_{n+1}I_n \rightarrow K_{n-1}I_n + 2$ K (red dashed line). Clearly, thicker layers of nonstoichiometric $K_{n+1}I_n$ would more strongly disfavor deintercalation and oxidation. The red curve in Fig. 3(b) is then vertically downshifted by μ_K in K_2O, K_2O_2, and KO_2 (μ_O taken from the energy of O_2) to yield the deintercalation penalties for these respective end states for K. The K_2O curve would be most relevant since it is the earliest state that the oxidation process has to pass through; it is downshifted relative to the top curve for K by $\frac{1}{2}E_{K_2O} - \frac{1}{4}E_{O_2} - E_K = -1.7$ eV, where the deintercalation energies are −1.5 and 0.5 eV for $n = 0$ and the large n asymptote, respectively. *Thus the presence of a salt backbone increases the deintercalation energy* (into K_2O) by 2.0 eV per K atom. This increased stability can be further enhanced by tuning thermochemical parameters, e.g., a higher system temperature would decrease the free energy of gas-phase O_2 and may thus disfavor oxidation, a well-known trend in extractive metallurgy [44], although here one must also factor in entropic contributions towards possible alkali volatilization. The excess iodine case (see Supplemental Material [23]) shows a similar trend of increasing stability with thicker salt slabs, with an asymptote of 0.9 eV.

Discussion.—The intercalant stabilization strategy proposed above should be generalizable to other interfaces [45,46], since it essentially relies on the increased energy penalty of extracting the species in excess (e.g., K) from the opposite-charge species (I). This strategy is to some extent a crystalline solid-state analog of ionic liquid gating, at what is likely the ultimate limit in the areal density of ionic excess, locked into a crystalline lattice structure. A carbon

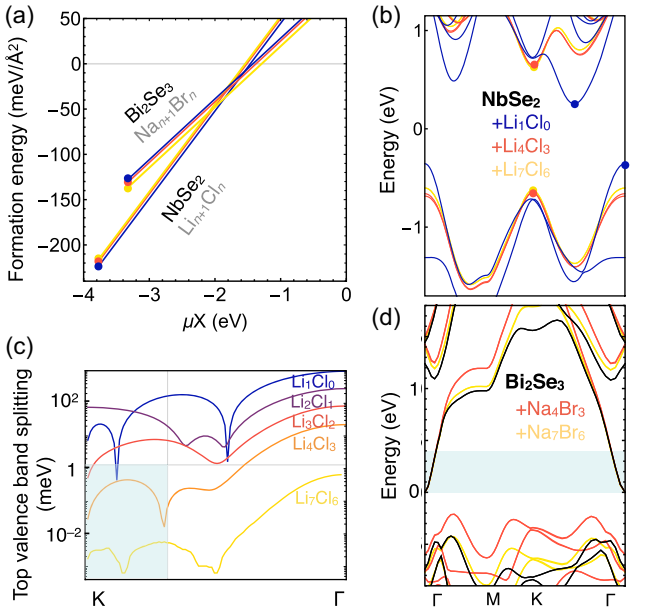

FIG. 4. (a) Formation energy for $NbSe_2$ and Bi_2Se_3 intercalated by salt with excess alkali. (b) Band structure of $NbSe_2 + Li_{n+1}Cl_n$ showing an indirect-to-direct transition (band edges in blue circles and red circles) when the intercalating salt becomes thicker than Li_4Cl_3. (c) Interlayer coupling in salt-intercalated $NbSe_2$ as k_F varies along the Γ-K direction. The gray horizontal line indicates the estimated upper limit of interlayer coupling that allows for Ising pairing. (d) Band structure of $Bi_2Se_3 + Na_{n+1}Br_n$, showing that the high Fermi velocity in the conduction band at Γ known to monolayer Bi_2Se_3 (black) is preserved in intercalated Bi_2Se_3 (colored). The blue region indicates the band dispersion magnitude in the out-of-plane direction for bulk Bi_2Se_3.

nanotube interior may be especially amenable to nonstoichiometric salt due to geometrical packing constraints, particularly if deposited with the nanotube held under electrical bias.

More broadly, salted intercalation should be agnostic to the layered material being doped, so long as its work function or electron affinity is sufficiently large (if alkali metal is in excess). Particularly interesting are layered materials where salted intercalation may yield a *bulk* phase with properties that are generally considered unique to monolayers, as the constituent layers are decoupled by the intervening salt slabs. For example, producing a MoS_2-like direct gap in a bulk layered phase, preserving Ising pairing in bulk $NbSe_2$, and potentially increasing the thermoelectric figure of merit in Bi_2Se_3. Similar to our analysis of salt-intercalated graphene, we first establish the thermodynamic stability of 2D layers paired with a nonstoichiometric salt and then show layer decoupling by analyzing electronic structures. Salts are again chosen to lattice-match the 2D layers for computational convenience: $NbSe_2$ is paired with $Li_{n+1}Cl_n$ and Bi_2Se_3 with $Na_{n+1}Br_n$ (details of the ground state search in Supplemental Material [23]). In Fig. 4(a), the formation energies of the two materials for $n = 0$, 3, 6 are again each nearly independent of n, indicating that complete charge transfer from the excess alkali dominates salt-layer interaction, independent of n. This behavior also reflects minimal lattice mismatch—e.g., if LiCl was strained to achieve the lattice match, then formation energies would increase with thicker salt layers due to increasing strain energy (not shown here).

Direct gap.— The direct gaps unique to monolayer Mo or W dichalcogenides could potentially be recovered in the bulk through salted intercalation into a related electron-deficient dichalcogenide. We consider $NbSe_2 + Li_{n+1}Cl_n$, where the electron deficiency of $NbSe_2$ both drives intercalation and makes the result isoelectronic to MoS_2. The band structures for $n = 0$, 3, 6 in Fig. 4(b) transition from indirect gap for Li_1Cl_0 (blue) to direct gaps in Li_4Cl_3 (red) and Li_7Cl_6 (yellow). This transition resembles the well-known indirect-to-direct transition in MoS_2 when interlayer interaction is removed, i.e., the system maintains isoelectronicity to MoS_2 in the presence of salt. With thicker salt layers, the indirect band edges (blue circles) retreat outside the K point direct gap (red and yellow circles), a behavior consistent with the increasing quantum confinement and decreasing band repulsion known to cause the indirect-to-direct transition in group-VIB transition metal dichalcogenides [47].

Ising pairing.—Another property unique to monolayer metals is 2D Ising superconductivity, in which the orbital limit of the upper critical field is relieved [48], allowing measurement of the paramagnetic limit, which is drastically increased by strong spin-orbit coupling in noncentrosymmetric monolayer $NbSe_2$ [49]. Relieving the orbital limit in *bulk* $NbSe_2$ requires an out-of-plane coherence length ξ_z smaller than the interlayer separation c, $\xi_z < c/\sqrt{2}$ [48,50,51], which is equivalent to the interlayer hopping being small compared to the superconducting gap (i.e., $\xi_z = \hbar v_F/\Delta \approx t_{\text{inter}} c/\pi\Delta < c/\sqrt{2} \rightarrow t_{\text{inter}} < \Delta\pi/\sqrt{2}$, where v_F is the Fermi velocity, Δ the superconducting gap, and t_{inter} the interlayer coupling near the Fermi level). Taking $\Delta = 0.6$ meV from bilayer $NbSe_2$ (the thinnest case for which a tunneling current could be detected in Ref. [52]) yields $t_{\text{inter}} < 1.3$ meV to achieve 2D behavior. Finally, t_{inter} in salt-intercalated $NbSe_2$ is calculated as the interlayer bonding-antibonding splitting (i.e., band dispersion magnitude along k_z on the K pocket) because the superconducting response to magnetic fields in $NbSe_2$ is dominated by the K pocket Fermi surface [49]. In Fig. 4(c), we plot t_{inter} as a function of the Fermi wave vector k_F along $\Gamma - K$. We use the $Li_{n+1}Cl_n$ calculation for this purpose, since the k_z bandwidths should be similar to those of a less-doped metallic case. k_F depends on the degree of charge transfer from the salt, and is confined within the left boundary ($NbSe_2$ fully compensated by lattice-matching salt) and the right boundary of the blue box ($NbSe_2$ lightly doped by large-lattice-constant salt, estimated from the Fermi surface of pristine $NbSe_2$). Thus

we find that $t_{\text{inter}} < 1.3$ meV is achieved near $n = 2$ and 3, where the $NbSe_2$ separations are 12–15 Å. This result is consistent with large in-plane upper critical fields seen in the misfit layered compound $(LaSe)_{1.14}(NbSe_2)_{1,2}$, where $NbSe_2$ layers are also separated at 12 Å and may be electronically decoupled [53].

Thermoelectrics.—For Bi_2Se_3, separating monolayers does not help in preserving bulk topological order (unlike intercalating monovalent metals [54]), but could be useful for thermoelectrics. A challenge in achieving high thermoelectric figure of merit ZT is maximizing the thermopower (Seeback coefficient) and electrical conductivity suffers a trade-off between these two quantities. This trade-off can be overcome by confining (relative to the thermal de Broglie wavelength [55]) materials to two or one dimensions, following Hick-Dresselhaus theory [56,57]. High ZT has thus been predicted or realized in monolayer Bi_2Se_3 [58], PbTe quantum wells [59,60], and bulk materials with highly anisotropic 2D-like band dispersions [61–63]. The large ZT in Bi_2Se_3 may not be entirely due to the Hick-Dresselhaus mechanism (since it assumes that bulk electronic structure persists in lower dimensions along the unconfined dimensions [64]), but the reverse process of assembling 2D Bi_2Se_3 into a quasi-2D intercalated 3D Bi_2Se_3 is easier to consider: given that a large ZT is known experimentally for n-type monolayer Bi_2Se_3, an intercalated 3D Bi_2Se_3 would retain a large ZT, provided that conduction band characteristics (e.g., large Fermi velocity and 2D-like density of states) remain after intercalation. In Fig. 4(d) we show that, after salt intercalation, the conduction band electronic structure of monolayer Bi_2Se_3 (black) is mostly preserved after $Na_{n+1}Br_n$ intercalation for $n > 3$ (red). The blue window indicates the magnitude of band dispersion along k_z in bulk Bi_2Se_3, 0.3 eV. By contrast, dispersion along k_z is negligible for Na_4Br_3 and Na_7Br_6, at 7 and 0.3 meV, respectively, and so would yield 2D-like band-edge densities of states. Overall, this suggests that intercalating 2D materials of high ZT may provide a way to realize high-ZT thermoelectrics in 3D bulk. Unlike the existing highly anisotropic materials that require ultrahigh vacuum conditions to synthesize [59,60], salt-intercalated Bi_2Se_3 may be synthesizable at scale.

In sum, "salted" intercalation of diverse layered materials may provide a general means to decouple 2D layers en masse and thus obtain monolayerlike properties in the bulk, while also converting semimetals like graphene into potentially air-stable systems, and 2D metals into semiconductors.

This work was supported by the Office of Science, Office of Basic Energy Sciences, Materials Sciences and Engineering Division of the Department of Energy under Contract No. DE-AC02-05-CH11231 within the Theory of Materials program (KC2301), the National Science Foundation through the 2-Dimensional Crystal Consortium, a Materials Innovation Platform under DMR-1539916 and DMR-2039351, and the Penn State Materials Research Science and Engineering Center under DMR-1420620 and DMR-2011839. M. L. C. support was also provided by NSF Grant No. DMR-1926004 for first-principles computations of the electronic structures. Computational resources were in part from the Department of Energy at Lawrence Berkeley National Laboratory, a NERSC facility. A. N. acknowledges startup funds from the University of Akron and Y. W. from the University of North Texas.

*nourhani@uakron.edu

[1] R. Tycko, G. Dabbagh, M. J. Rosseinsky, D. W. Murphy, R. M. Fleming, A. P. Ramirez, and J. C. Tully, Science **253**, 884 (1991).
[2] Y. Iwasa, K. Tanaka, T. Yasuda, T. Koda, and S. Koda, Phys. Rev. Lett. **69**, 2284 (1992).
[3] T. Pichler, M. Knupfer, M. S. Golden, J. Fink, J. Winter, M. Haluska, H. Kuzmany, M. Keshavarz-K, C. Bellavia-Lund, A. Sastre, J. C. Hummelen, and F. Wudl, Appl. Phys. A **64**, 301 (1997).
[4] V. Derycke, R. Martel, J. Appenzeller, and P. Avouris, Nano Lett. **1**, 453 (2001).
[5] J. Kong, C. Zhou, E. Yenilmez, and H. Dai, Appl. Phys. Lett. **77**, 3977 (2000).
[6] M. A. Py and R. R. Haering, Can. J. Phys. **61**, 76 (1983).
[7] F. Xiong, H. Wang, X. Liu, J. Sun, M. Brongersma, E. Pop, and Y. Cui, Nano Lett. **15**, 6777 (2015).
[8] B. M. Ludbrook, G. Levy, P. Nigge, M. Zonno, M. Schneider, D. J. Dvorak, C. N. Veenstra, S. Zhdanovich, D. Wong, P. Dosanjh, C. Straßer, A. Stöhr, S. Forti, C. R. Ast, U. Starke, and A. Damascelli, Proc. Natl. Acad. Sci. U.S.A. **112**, 11795 (2015).
[9] M. S. Dresselhaus and G. Dresselhaus, Adv. Phys. **30**, 139 (1981).
[10] Y. Koike, S. ichi Tanuma, H. Suematsu, and K. Higuchi, J. Phys. Chem. Solids **41**, 1111 (1980).
[11] P. Stephens, L. Mihaly, P. Lee, R. Whetten, S. Huang, R. Kaner, F. Deiderich, and K. Holczer, Nature (London) **351**, 632 (1991).
[12] T. W. Ebbesen, J. S. Tsai, K. Tanigaki, J. Tabuchi, Y. Shimakawa, Y. Kubo, I. Hirosawa, and J. Mizuki, Nature (London) **355**, 620 (1992).
[13] R. S. Lee, H. J. Kim, J. E. Fischer, A. Thess, and R. E. Smalley, Nature (London) **388**, 255 (1997).
[14] Y. Wang, J. Xiao, H. Zhu, Y. Li, Y. Alsaid, K. Y. Fong, Y. Zhou, S. Wang, W. Shi, Y. Wang, A. Zettl, E. J. Reed, and X. Zhang, Nature (London) **550**, 487 (2017).
[15] N. Akuzawa, T. Amemiya, and Y. Takahashi, Carbon **24**, 295 (1986).
[16] N. Akuzawa, T. Fujisawa, T. Amemiya, and Y. Takahashi, Synth. Met. **7**, 57 (1983).
[17] Z. H. Pan, J. Camacho, M. H. Upton, A. V. Fedorov, C. A. Howard, M. Ellerby, and T. Valla, Phys. Rev. Lett. **106**, 187002 (2011).

[18] J. Sloan, S. Friedrichs, R. R. Meyer, A. I. Kirkland, J. L. Hutchison, and M. L. Green, Inorg. Chim. Acta **330**, 1 (2002).

[19] A. G. Kvashnin, P. B. Sorokin, and D. Tománek, J. Phys. Chem. Lett. **5**, 4014 (2014).

[20] P. B. Sorokin, A. G. Kvashnin, Z. Zhu, and D. Tománek, Nano Lett. **14**, 7126 (2014).

[21] J. Goniakowski, C. Noguera, and L. Giordano, Phys. Rev. Lett. **98**, 205701 (2007).

[22] C. L. Freeman, F. Claeyssens, N. L. Allan, and J. H. Harding, Phys. Rev. Lett. **96**, 066102 (2006).

[23] See Supplemental Material at http://link.aps.org/supplemental/10.1103/PhysRevLett.129.266401 for details of density functional theory calculations, all competing phases considered in Fig. 2, structural approximations for incommensurate salt-intercalated graphene systems, intercalation involving excess iodine, reverse encapsulation, NaCl intercalation, and structure of salt-intercalated layered chalcogenide systems. The Supplemental Material includes Refs. [24–39].

[24] J. P. Perdew, K. Burke, and M. Ernzerhof, Phys. Rev. Lett. **77**, 3865 (1996).

[25] S. Grimme, J. Antony, S. Ehrlich, and H. Krieg, J. Chem. Phys. **132**, 154104 (2010).

[26] J. Neugebauer and M. Scheffler, Phys. Rev. B **46**, 16067 (1992).

[27] R. A. Hoyt, E. M. Remillard, E. D. Cubuk, C. D. Vecitis, and E. Kaxiras, J. Phys. Chem. C **121**, 609 (2017).

[28] E. R. Margine and V. H. Crespi, Phys. Rev. Lett. **96**, 196803 (2006).

[29] S. Okada, A. Oshiyama, and S. Saito, Phys. Rev. B **62**, 7634 (2000).

[30] M. Posternak, A. Baldereschi, A. J. Freeman, E. Wimmer, and M. Weinert, Phys. Rev. Lett. **50**, 761 (1983).

[31] J. L. McChesney, A. Bostwick, T. Ohta, T. Seyller, K. Horn, J. González, and E. Rotenberg, Phys. Rev. Lett. **104**, 136803 (2010).

[32] R. Nandkishore, L. S. Levitov, and A. V. Chubukov, Nat. Phys. **8**, 158 (2012).

[33] J.-J. Zheng and E. R. Margine, Phys. Rev. B **94**, 064509 (2016).

[34] G. Profeta, M. Calandra, and F. Mauri, Nat. Phys. **8**, 131 (2012).

[35] A. Sanna, G. Profeta, A. Floris, A. Marini, E. K. U. Gross, and S. Massidda, Phys. Rev. B **75**, 020511(R) (2007).

[36] E. R. Margine, H. Lambert, and F. Giustino, Sci. Rep. **6**, 21414 (2016).

[37] G. Shi, L. Chen, Y. Yang, D. Li, Z. Qian, S. Liang, L. Yan, L. H. Li, M. Wu, and H. Fang, Nat. Chem. **10**, 776 (2018).

[38] W. Hebenstreit, M. Schmid, J. Redinger, R. Podloucky, and P. Varga, Phys. Rev. Lett. **85**, 5376 (2000).

[39] Y. Liu, B. V. Merinov, and W. A. Goddard, Proc. Natl. Acad. Sci. U.S.A. **113**, 3735 (2016).

[40] R. R. Meyer, J. Sloan, R. E. Dunin-Borkowski, A. I. Kirkland, M. C. Novotny, S. R. Bailey, J. L. Hutchison, and M. L. H. Green, Science **289**, 1324 (2000).

[41] R. Senga, H.-P. Komsa, Z. Liu, K. Hirose-Takai, A. V. Krasheninnikov, and K. Suenaga, Nat. Mater. **13**, 1050 (2014).

[42] C. Hérold, A. Hérold, and P. Lagrange, Solid State Sci. **6**, 125 (2004).

[43] V. Mordkovich, Y. Ohki, S. Yoshimura, S. Hino, T. Yamashita, and T. Enoki, Synth. Met. **68**, 79 (1994).

[44] H. J. T. Ellingham, J. Soc. Chem. Ind. **63**, 125 (1944).

[45] J. Goniakowski, C. Noguera, and L. Giordano, Phys. Rev. Lett. **93**, 215702 (2004).

[46] J. Goniakowski and C. Noguera, Phys. Rev. B **66**, 085417 (2002).

[47] L. Zhang and A. Zunger, Nano Lett. **15**, 949 (2015).

[48] M. Tinkham, *Introduction to Superconductivity: Second Edition*, Dover Books on Physics (Dover Publications, New York, 2004).

[49] X. Xi, Z. Wang, W. Zhao, J.-H. H. Park, K. T. Law, H. Berger, L. Forró, J. Shan, and K. F. Mak, Nat. Phys. **12**, 139 (2016).

[50] S. T. Ruggiero, T. W. Barbee, and M. R. Beasley, Phys. Rev. Lett. **45**, 1299 (1980).

[51] R. A. Klemm, A. Luther, and M. R. Beasley, Phys. Rev. B **12**, 877 (1975).

[52] E. Khestanova, J. Birkbeck, M. Zhu, Y. Cao, G. L. Yu, D. Ghazaryan, J. Yin, H. Berger, L. Forró, T. Taniguchi, K. Watanabe, R. V. Gorbachev, A. Mishchenko, A. K. Geim, and I. V. Grigorieva, Nano Lett. **18**, 2623 (2018).

[53] P. Samuely, P. Szabó, J. Kačmarčík, A. Meerschaut, L. Cario, A. G. M. Jansen, T. Cren, M. Kuzmiak, O. Šofranko, and T. Samuely, Phys. Rev. B **104**, 224507 (2021).

[54] Y. S. Hor, A. J. Williams, J. G. Checkelsky, P. Roushan, J. Seo, Q. Xu, H. W. Zandbergen, A. Yazdani, N. P. Ong, and R. J. Cava, Phys. Rev. Lett. **104**, 057001 (2010).

[55] N. T. Hung, E. H. Hasdeo, A. R. T. Nugraha, M. S. Dresselhaus, and R. Saito, Phys. Rev. Lett. **117**, 036602 (2016).

[56] L. D. Hicks and M. S. Dresselhaus, Phys. Rev. B **47**, 16631 (1993).

[57] L. D. Hicks and M. S. Dresselhaus, Phys. Rev. B **47**, 12727 (1993).

[58] Y. Sun, H. Cheng, S. Gao, Q. Liu, Z. Sun, C. Xiao, C. Wu, S. Wei, and Y. Xie, J. Am. Chem. Soc. **134**, 20294 (2012).

[59] L. D. Hicks, T. C. Harman, X. Sun, and M. S. Dresselhaus, Phys. Rev. B **53**, R10493 (1996).

[60] T. C. Harman, D. L. Spears, and M. J. Manfra, J. Electron. Mater. **25**, 1121 (1996).

[61] D. I. Bilc, G. Hautier, D. Waroquiers, G. M. Rignanese, and P. Ghosez, Phys. Rev. Lett. **114**, 136601 (2015).

[62] D. Parker, X. Chen, and D. J. Singh, Phys. Rev. Lett. **110**, 146601 (2013).

[63] A. Li, C. Hu, B. He, M. Yao, C. Fu, Y. Wang, X. Zhao, C. Felser, and T. Zhu, Nat. Commun. **12**, 5408 (2021).

[64] S. Urazhdin, D. Bilc, S. D. Mahanti, S. H. Tessmer, T. Kyratsi, and M. G. Kanatzidis, Phys. Rev. B **69**, 085313 (2004).